

# Shakedown analysis of pressure pipeline with an oblique nozzle at elevated temperatures using the Linear Matching Method

Jian-Guo Gong<sup>1</sup>, Tian-Ye Niu<sup>1</sup>, Haofeng Chen<sup>2,\*</sup>, Fu-Zhen Xuan<sup>1,\*</sup>

\*Corresponding authors.

E-mail: haofeng.chen@strath.ac.uk (Haofeng Chen); fzxuan@ecust.edu.cn (Fu-Zhen Xuan)

*(1. School of Mechanical and Power Engineering, East China University of Science and Technology, Shanghai 200237, China; 2. Department of Mechanical & Aerospace Engineering, University of Strathclyde, James Weir Building, 75 Montrose Street, Glasgow, G1 1XJ, UK)*

**Abstract:** There are many power plant components operating at elevated temperatures, subjected to the combined mechanical and thermal loading conditions. The shakedown problem is an important topic for the safe operation of these high temperature components. This work mainly addresses the shakedown analysis of the pressure pipeline with an oblique nozzle at elevated temperatures using the Linear Matching Method (LMM). Parametric studies on main factors affecting the shakedown boundary are conducted. The results indicate that the LMM analysis tool is adequate to identify the shakedown boundary of the component, verified by the ABAQUS step-by-step analysis. Regarding to the angle of the oblique nozzle, the ratchet limit is enhanced with the increasing angle, while the reverse plasticity limit increases until a maximum value is reached, and then presents a certain decrease. This implies that designers should make some compromises on the limit load and reverse plasticity limit when determining an economic angel of the oblique nozzle. In addition, parametric studies demonstrate that the diameter-to-thickness ratios of the oblique nozzle and the main pipe have a remarkable effect on the reverse plasticity and ratchet limit of the component.

**Keywords:** Linear Matching Method (LMM); Oblique nozzle; Structural integrity; Shakedown

## 1 Introduction

Pressure pipelines are widely used for fluid transportation and other industrial applications in many fields, such as the petrochemical engineering, nuclear engineering, and so on. Due to the requirements of the process design and the limitation of the installation, an oblique nozzle is necessary for some occasions. Compared with an orthogonal nozzle, an oblique nozzle can induce a much higher stress and strain distribution with the same loading and geometrical conditions. In general, the pipelines are subjected to the varying mechanical loading (e.g. internal pressure) and thermal gradient (e.g. temperature difference across the thickness), etc. Under such complex condition, on one hand, the component may present accumulated plastic strain with the increasing cycles, namely, the ratchetting behavior, inducing the incremental collapse of the component. On the other hand, the component can also indicate the reverse plasticity under the cyclic thermal-mechanical loadings. Therefore, to avoid the structural failure by the ratcheting behavior or the low cycle fatigue due to the reverse plasticity mechanism, it is essential to predict the shakedown boundary of the pressure pipeline with an oblique nozzle.

Generally speaking, it is very difficult to gain the analytical solutions for the shakedown limit for a practical engineering structure due to the complexity of the geometry of the structure, loading conditions, and so on. An alternative method for solving such difficulty is the incremental finite element analysis, which has been widely used by many researchers in dealing with various applications. The challenging issues for the incremental finite element analysis include two aspects: One is that this FEA method is based on the step-by-step strategy, implying a huge computation effort, especially for complex engineering components. The other aspect is that a significant number of trial and error case studies are needed for identifying the shakedown limit of a given component. Combining with the above two aspects, it can be expected that the incremental finite element analysis could be very time-consuming. Based on the above limitations, it is vital to explore advanced direct methods for the shakedown limit analysis of practical components with reduced computation efforts.

In the past decades, some direct methods have been proposed based on Koiter's kinematic and the Melan's static theorems [1-2], such as the nonlinear superposition method [3], mathematical

programming methods [4-5], the generalized local stress strain (GLOSS) r-node method [6], the elastic compensation method (ECM) [7-8], the linear matching method (LMM) [9-17], and so on. As a whole, the above methods have achieved some success in different engineering applications. In this work, the LMM framework is a main concern due to the advantage of satisfaction of the equilibrium and compatibility in each increment. Some previous studies of the authors have demonstrated the accurate prediction of the advanced direct method with different components included for analyses, such as plates with a hole [9, 13-14], pipeline with a part-through slot [9], tubeplate of the superheater header [12], pipe with two parallel branch pipes [15-16], metal matrix composite (MMC) [17], and so on. Considering the complex and high stress/strain distribution of the pressure pipe with an oblique nozzle, the application of the latest LMM analysis tool to shakedown boundary of such a complex structure with an oblique nozzle will be addressed in this work.

The structure of this paper is arranged as follows: Firstly, the LMM framework for shakedown analysis is given in Section 2. Secondly, the finite element model of the pressure pipeline with an oblique nozzle is provided in Section 3. Thirdly, verifications by the ABAQUS step-by-step analysis for the shakedown analysis are provided and the parametric studies on main factors affecting the shakedown boundary are shown in Section 4. Finally, conclusions drawn through investigations of this work are summarized in Section 5.

## 2 LMM framework for shakedown and ratchet analysis

The material studied here is isotropic, elastic-perfectly plastic and satisfies the von Mises yield condition. Regarding a body of volume,  $V$ , with a surface area  $S$ , it is subjected to varying mechanical loads,  $\lambda_p P(x_i, t)$  over the surface area,  $S_p$ , and varying thermal loads  $\lambda_\theta \theta^V(x_i, t)$ . A zero displacement rate condition is applied over the remainder of the surface area,  $S_u$  such that  $\dot{u}_i = 0$ .

The corresponding linear elastic stress history can be expressed as Eq. (1):

$$\hat{\sigma}_{ij}(x_k, t) = \lambda_p \hat{\sigma}_{ij}^P(x_k, t) + \lambda_\theta \hat{\sigma}_{ij}^\theta(x_k, t) \quad (1)$$

where,  $\hat{\sigma}_{ij}^P(x_k, t)$  and  $\hat{\sigma}_{ij}^\theta(x_k, t)$  are the elastic stress histories corresponding to  $P(x_k, t)$  and

$\theta(x_k, t)$ , respectively. Over a time cycle  $0 \leq t \leq t_0$ , the stress and strain rates will asymptote to a cyclic state where

$$\sigma_{ij}(t) = \sigma_{ij}(t + \Delta t), \dot{\epsilon}_{ij}(t) = \dot{\epsilon}_{ij}(t + \Delta t) \quad (2)$$

The cyclic stress history  $\sigma_{ij}(x_k, t)$  over a given time cycle is given as Eq. (3):

$$\sigma_{ij}(x_k, t) = \lambda_0 \hat{\sigma}_{ij}(x_k, t) + \bar{\rho}_{ij}(x_k) + \rho_{ij}^r(x_k, t) \quad (3)$$

where,  $\lambda_0$  is a load multiplier.  $\bar{\rho}_{ij}(x_k)$  is a constant residual stress and corresponds to the constant part of  $\lambda_0 \hat{\sigma}_{ij}(x_k, t)$ .  $\rho_{ij}^r(x_k, t)$  is a changing residual stress corresponding to the changing part of  $\lambda_0 \hat{\sigma}_{ij}(x_k, t)$  during a cycle, satisfying the requirement of Eq. (4):

$$\rho_{ij}^r(x_k, 0) = \rho_{ij}^r(x_k, \Delta t) = \bar{\rho}_{ij}^0(x_k) \quad (4)$$

where,  $\bar{\rho}_{ij}^0(x_k)$  is the constant element of  $\rho_{ij}^r$ .

The LMM numerical procedures for the shakedown and ratchet analyses have been reported by Chen et al. [18]. Regarding a general cyclic load, it can be divided into the constant and cyclic components. The solution of the shakedown limit only includes a global minimization process to evaluate the constant residual stress caused by the combined action of the cyclic and constant loadings. The determination of the ratchet limit is implemented by a two stage nonlinear minimization procedure: The first step is to compute a changing residual stress  $\rho_{ij}^r$  by an incremental minimization of the energy function with the application of the cyclic load; The second step is to perform a global minimization of the upper bound shakedown theorem and to evaluate the ratchet limit for an additional constant load, where the cyclic linear elastic solution is augmented by the changing residual stress field  $\rho_{ij}^r$  obtained in the first step.

Consider an energy function

$$I(\dot{\epsilon}_{ij}^c, \lambda) = \int \int_V (\sigma_{ij}^c - \sigma_{ij}) \dot{\epsilon}_{ij}^c dt dV \quad (5)$$

where,  $\dot{\epsilon}_{ij}^c$  is a kinematically admissible strain rate.  $\sigma_{ij}^c$  represents a stress at yield corresponding

to  $\dot{\varepsilon}_{ij}^c$ .

## 2.1 Shakedown analysis

Regarding the shakedown analysis, the variable  $\rho_{ij}^r(x_k, t)$  need be equal to zero (see Eqs. (3) and (4)). Based on the shakedown conditions and a global minimization process of energy function, an inequality can be indicated as Eqs. (6)-(7).

$$I(\dot{\varepsilon}_{ij}^c, \lambda) = \sum_{k=1}^K I_k = \int_V \sum_{k=1}^K (\sigma_{ij}^k - \lambda(\hat{\sigma}_{ij}^k(t_k))) \Delta \varepsilon_{ij}^k dV \geq 0 \quad (6)$$

$$i.e. \quad \lambda \leq \frac{\int_V \sum_{k=1}^K \sigma_{ij}^k \Delta \varepsilon_{ij}^k dV}{\int_V \sum_{k=1}^K (\hat{\sigma}_{ij}^k(t_k)) \Delta \varepsilon_{ij}^k dV} = \frac{\int_V \sigma_y \sum_{k=1}^K \bar{\varepsilon}(\Delta \varepsilon_{ij}^k) dV}{\int_V \sum_{k=1}^K (\hat{\sigma}_{ij}^k(t_k)) \Delta \varepsilon_{ij}^k dV} = \lambda_{UB} \quad (7)$$

where,  $\Delta \varepsilon_{ij}^k$  is the strain increment at the time point  $t_k$ ,  $\sigma_y$  is the yield stress,  $\bar{\varepsilon}$  stands for the von Mises effective strain. It should be noted that the upper bound shakedown multiplier  $\lambda_{UB}$  can converge to the least bound limit  $\lambda$  through a number of iterations. The linear matching method adopts the convergence criterion that the difference of the upper bound for five consecutive iterations should be less than 0.1%.

If the combined elastic stress and a constant residual stress field do not violate the yield condition at any point, the component will shakedown. This implies that the lower bound of shakedown limit can be achieved based on Eq. (8) at all integration points.

$$f(\lambda_{LB} \hat{\sigma}_{ij}^r(x_k, t) + \bar{\rho}_{ij}^r(x_k)) \leq 0 \quad (8)$$

where,  $\lambda_{LB}$  is the lower bound shakedown multiplier.

## 2.2 Ratchet analysis

As mentioned above, the first step for ratchet analysis involves the solution of the changing residual stress field, which can be implemented by the direct steady cycle analysis (DSCA) of the LMM tool. This procedure is mainly concerned with the calculation of the accumulated residual stress history, which can be attributed to the history of the changing plastic strain induced by the cyclic loads. The constant residual stress  $\bar{\rho}_{ij}^r$  can be calculated as Eq. (9) by calculating the

varying residual stress  $\Delta\rho_{ij}^r(x_k, t_n)_m$ , corresponding to the elastic stress solution  $\sigma_{ij}^\Delta(x_k, t_n)$ .

$$\bar{\rho}_{ij}^r = \sum_{m=1}^M \sum_{n=1}^N \Delta\rho_{ij}^r(x_k, t_n)_m \quad (9)$$

where,  $m$  is the number of iterative sub-cycles, equal to 1 to  $M$ .  $n$  is the number of time instances for the applied load cycle, equal to 1 to  $N$ .

Then, the changing residual stress  $\rho_{ij}^r$  at the steady state cycle can be described by Eq. (10).

$$\rho_{ij}^r(x_k, t_n) = \bar{\rho}_{ij}^r(x_k) + \sum_{a=1}^n \Delta\rho_{ij}^r(x_k, t_a)_M \quad (10)$$

The corresponding converged increment of plastic strain at time  $t_n$  is given by Eq. (11).

$$\Delta\varepsilon_{ij}^p(x_k, t_n) = \Delta\varepsilon_{ij}^{p'}(x_k, t_n) = \frac{1}{2\bar{\mu}_n(x_k, t_n)} \left[ \sigma_{ij}^\Delta(x_k, t_n) + \rho_{ij}^r(x_k, t_n) \right] \quad (11)$$

where,  $\bar{\mu}_n$  is the iterative shear modulus identified by the linear matching method.  $\sigma_{ij}^\Delta$  is the linear elastic stress history. The notation ( $'$ ) refers to the deviator component of the stress and strain.

Regarding the ratchet analysis, the ratchet limit can be determined by the minimization of the upper bound shakedown theorem, with the elastic solution augmented by the changing residual stress  $\rho_{ij}^r(t_k)$ . The theorem gives

$$\int_V \sum_{k=1}^K \sigma_{ij}(t_k) \Delta\varepsilon_{ij}(t_k) dV = \int_V \sum_{k=1}^K \sigma_{ij}^c(t_k) \Delta\varepsilon_{ij}(t_k) dV \quad (12)$$

Using von Mises yield criterion, the following Eq. (13) can be gained.

$$\int_V \sum_{k=1}^K \sigma_{ij}^c(t_k) \Delta\varepsilon_{ij}(t_k) dV = \int_V \sum_{k=1}^K \sigma_y \bar{\varepsilon}(\Delta\varepsilon_{ij}(t_k)) dV \quad (13)$$

Then, an upper bound multiplier for ratchet limit can be found, shown as Eq. (14):

$$\lambda = \frac{\int_V \sum_{k=1}^K \sigma_y \bar{\varepsilon}(\Delta\varepsilon_{ij}(t_k)) dV - \int_V \sum_{k=1}^K (\sigma_{ij}^p(t_k) + \sigma_{ij}^\theta(t_k) + \rho_{ij}^r(t_k)) \Delta\varepsilon_{ij}(t_k) dV}{\int_V \sum_{k=1}^K \bar{\sigma}_{ij}(t_k) \Delta\varepsilon_{ij}(t_k) dV} \quad (14)$$

where, the multiplier  $\lambda$  gives the capacity of the body subjected to cyclic loads  $P$  and  $\theta$  to withstand constant loads  $\bar{P}$  and  $\bar{\theta}$  with no ratcheting behavior. Based on this framework, the LMM

produces monotonically reducing upper bounds, converging to the least upper bound ratchet limit for the chosen class of displacement fields. As those for shakedown analysis, the linear matching method adopts the convergence criterion that the difference of the upper bound for five consecutive iterations should be less than 0.1%.

### 3 Finite element model

#### 3.1 Geometrical model and mesh arrangement

The model taken for analysis is the pressure pipeline with an oblique nozzle, displayed in Fig. 1a and Fig. 1b. As shown in Fig. 1b, the angle of the oblique nozzle ( $\varphi_0$ ) was defined as the acute angle between the main pipe and the oblique nozzle. The main geometrical parameters of the model are given in Table 1. Considering the symmetry of the model, one-half model was established using the ABAQUS CAE [19]. The 20-node quadratic brick, reduced integration, hourglass control element C3D20R was adopted. The finite element model for the pressure pipeline with an oblique nozzle at elevated temperature, composed of 8,416 elements and 45,812 nodes, was illustrated in Fig. 1a. In the present work, the model was assumed to suffer from a cyclic temperature difference  $\Delta\theta$  between the internal and external surfaces of the component (see Fig. 1) and a constant internal pressure  $p$ . For simplification, the temperature outside the pressure pipeline was assumed as  $\theta_0=0$ .

Table 1 Main geometrical parameters of pressure pipeline with an oblique nozzle

Component	Parameters	Value
Pressure pipeline	Diameter $D_p$ (mm)	349
	Thickness $t_p$ (mm)	20
Oblique nozzle	Angle $\varphi_0$ ( $^\circ$ )	60
	Diameter $D_z$ (mm)	219
	Thickness $t_z$ (mm)	10
Fillet weld	Radius $R$ (mm) (outside)	10
	Radius $r$ (mm) (inside)	5

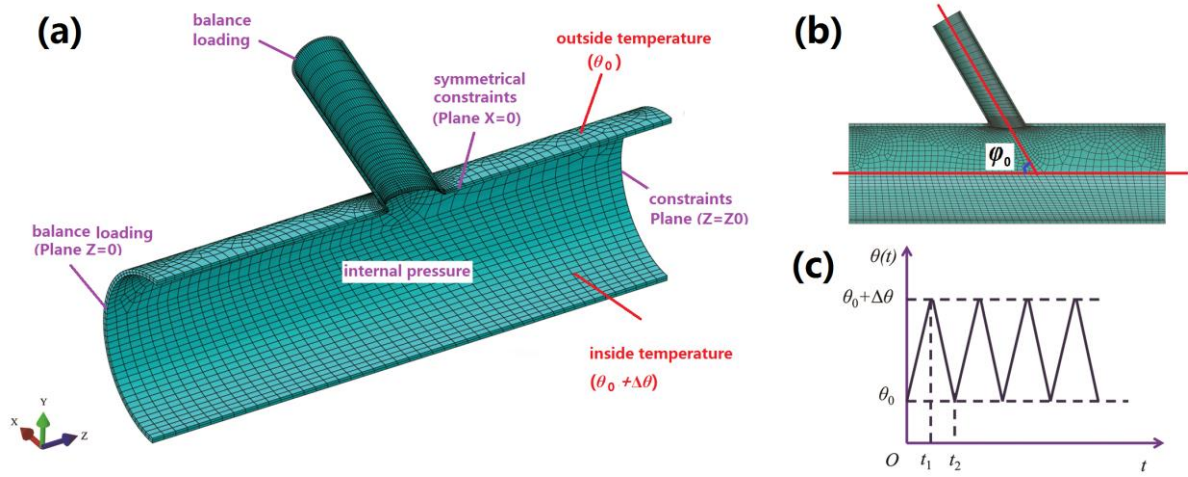


Fig. 1 Finite element model of pressure pipeline with an oblique nozzle at elevated temperature

### 3.2 Boundary conditions and material properties

The main boundary conditions of the finite element model were as follows (see Fig. 1): (1) The symmetrical constraints were imposed on the cutting plane  $X=0$  of the model; (2) The right cutting plane of the main pipe with the normal of  $Z$ -direction (Plane  $Z=Z_0$ ) was restrained; (3) The balance loadings were implied to the cutting plane of the oblique nozzle, as well as the left cutting plane of the main pipe with the normal of  $Z$ -direction (Plane  $Z=0$ ), determined by Eq. (15).

$$\sigma_{bl} = \frac{pD_i^2}{(D_o^2 - D_i^2)} \quad (15)$$

where,  $\sigma_{bl}$  is the balance loading (tensile stress);  $p$  is the internal pressure;  $D_i$  and  $D_o$  are internal and external diameters of the main and the branch pipes, respectively.

The material properties of the model [15-16, 20] were assumed as a stainless steel. The main elasto-plastic material properties are as follows: elastic modulus  $E=190\text{GPa}$ , the Poisson's ratio  $\mu=0.3$ . Temperature dependent yield stress ( $\sigma_y$ ) for the material studied is shown in Fig. 2. Thermal properties of the material are listed below: thermal conductivity  $k=1.63 \times 10^{-2} \text{ W/(m } ^\circ\text{C)}$  and the coefficient of thermal expansion  $\alpha=1.60 \times 10^{-5}$ . It should be noticed that an elastic-perfectly plastic (EPP) material model was adopted to identify the shakedown boundary, i.e. the Bree-like diagram [21], for each case study.

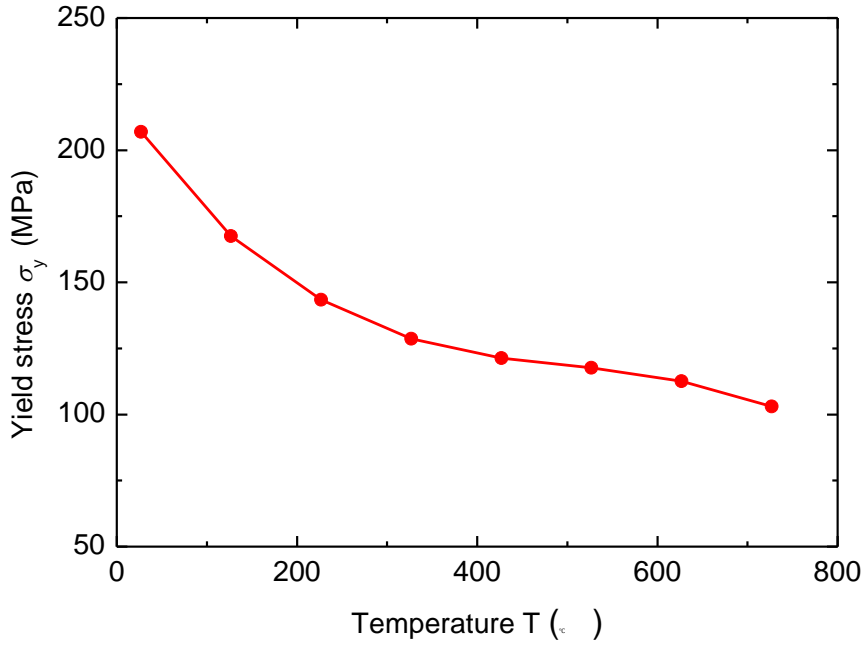


Fig. 2 Temperature dependent yield stress ( $\sigma_y$ ) for the material studied

## 4 Results and discussion

### 4.1 Bree-like diagram for pressure pipeline with an oblique nozzle

To have an entire view of the cyclic behavior of the component, the Bree-like diagram, i.e. the shakedown and ratchet limit interaction curves, of the pressure pipeline with an oblique nozzle are provided in Fig. 3. It is worth noting that the main focus in following Sections 4.2 and 4.3 is the shakedown limit interaction curve. As shown in Fig. 3, a normalized internal pressure ( $p/p_{lim}$ ) and a temperature range ( $\Delta\theta/\Delta\theta_0$ ) are chosen as the abscissa and the ordinate, respectively. Herein, the reference temperature is  $\Delta\theta_0=100^\circ\text{C}$  and the reference internal pressure is  $p_{lim}=9.369\text{MPa}$ , which is the limit internal pressure. There are three different kinds of failure mechanisms in the Bree-like diagram: shakedown, reverse plasticity and ratcheting behavior, and these three failure mechanisms are also marked in Fig. 3.

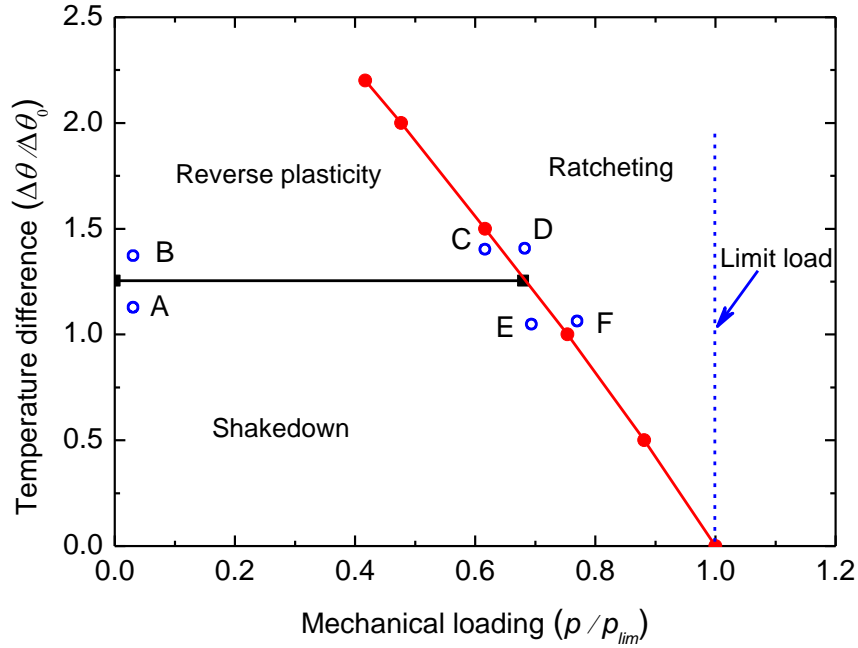


Fig. 3 Bree-like diagram for pressure pipeline with an oblique nozzle under varying internal pressure and temperature difference

The effective plastic strain distributions normalized to the maximum value for the component under the pure mechanical load case (i.e. the limit load) and under the cyclic thermal loading condition only (i.e. the reverse plasticity limit) are displayed in Fig. 4, respectively. This is mainly because the optimization of the upper bound shakedown theorem results in a distribution of strain of arbitrary magnitude. The upper bound is independent of the overall size of the strain field but is dependent on the spatial distribution. Regarding the pure mechanical load case (see Fig. 4a), the main plastic strain is concentrated at the joint between the main pipe and the nozzle, parallel to the axis of the main pipe. For the pure cyclic thermal loading condition, the maximum effective plastic strain is located at the joint between the main pipe and the oblique nozzle, which deviates from the central axis of the main pipe with a certain angle of  $\alpha$  (see Fig. 4b). It should be noted that the main difference of plastic strain distribution between limit load case and reverse plasticity case is that the limit load case shows a global failure mechanism, a complete yielding through the pipe wall, while the reverse plasticity exhibits a local failure mechanism, associated with the Low Cycle Fatigue (LCF).

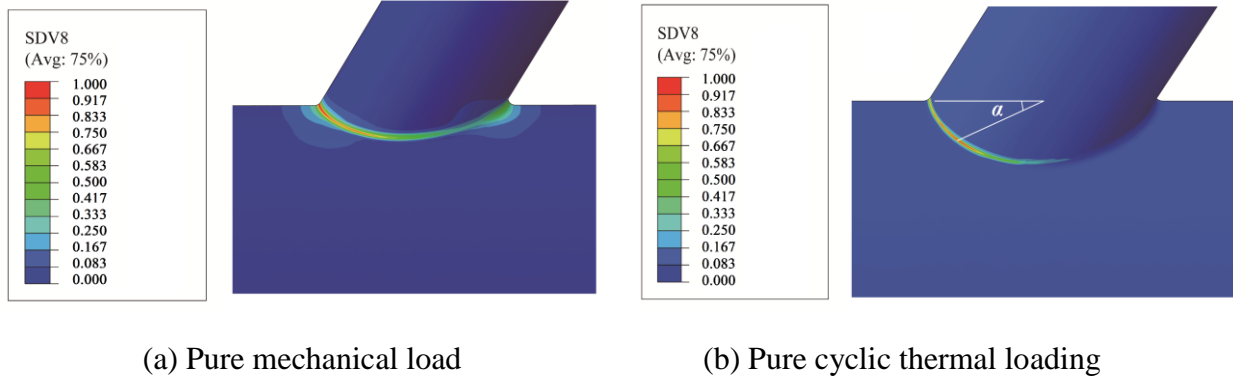
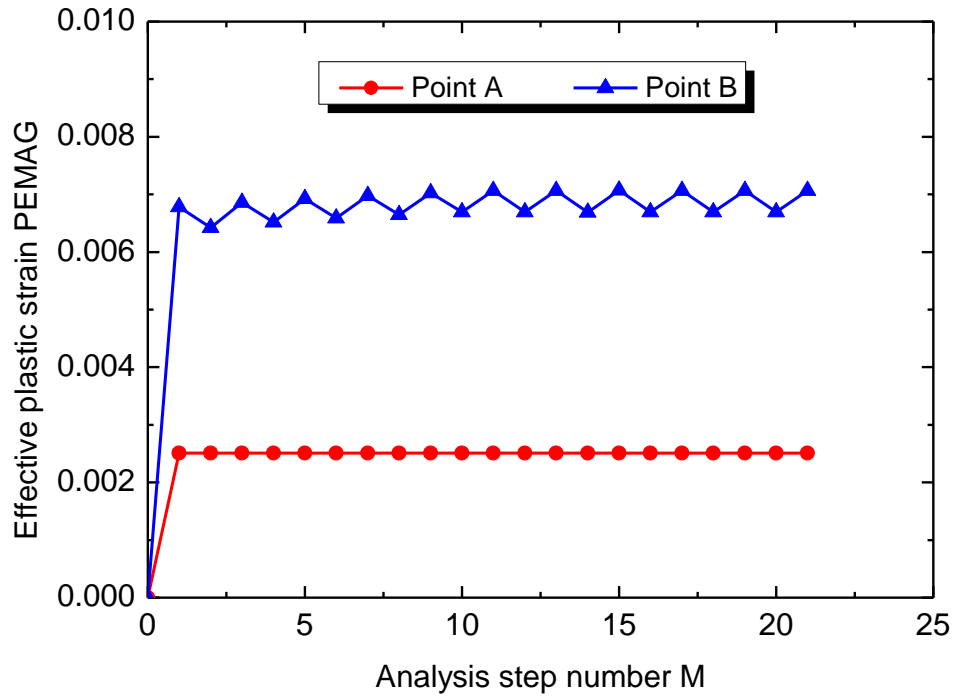


Fig. 4 Effective plastic strain distributions under pure mechanical and pure thermal loadings

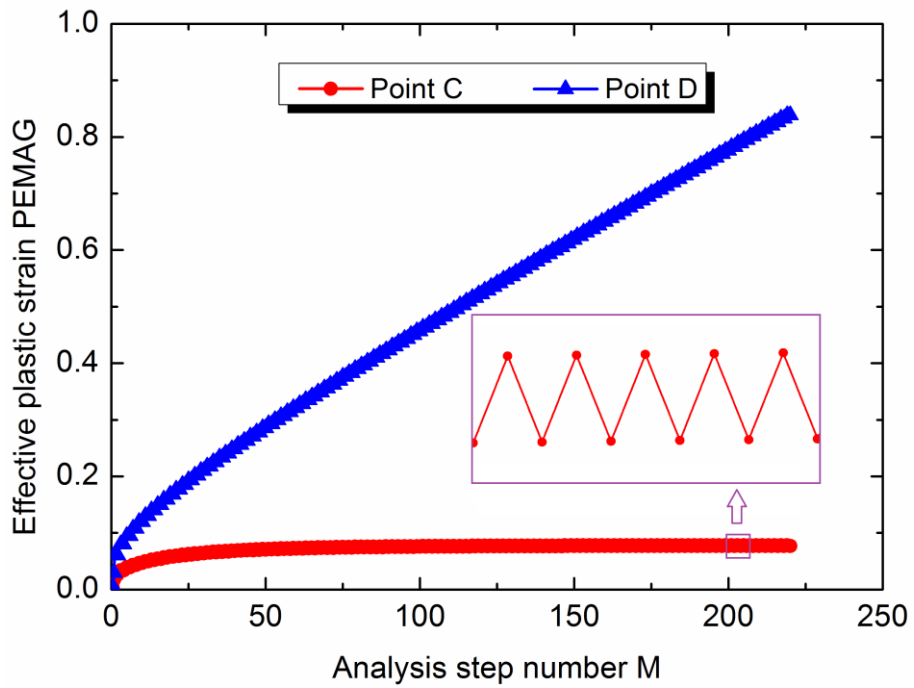
To verify the numerical results based on the LMM plugin, the ABAQUS step-by-step analysis is conducted. Several points (Points A, B, C, D, E and F in Fig. 3), corresponding to various loading combinations, are selected as reference points.

Regarding Points A and B close to the reverse plasticity limit, the effective plastic strain curves along with the number of the analysis step are displayed in Fig. 5a. For Load Case A, there is no further increase of the effective plastic strain after the initial plastic strain, while the stable reverse plasticity behavior is observed for Load Case B. It should be noted that for the reverse plasticity limit, it is located at the place that the von Mises value of the variation of the effective elastic stress reaches twice the yield stress, which usually occurs at a single point. Regarding Points C and D close to the ratchet limit, the effective plastic strain curves along with the number of cycles are displayed in Fig. 5b. Regarding Load Case C, the stable reverse plasticity behavior is observed after reaching the steady state cycle, while the ratcheting behavior of component can be seen for Load Case D. Regarding Points E and F close to the ratchet limit curve, as given in Fig. 5c, there is no further increase of the effective plastic strain after reaching the steady state cycle for Load Case E, demonstrating a shakedown mechanism, while the ratcheting behavior of the component is clearly observed for Load Case F. It should be noted that different from the reverse plasticity limit, the ratchet limit converges to a strain field that corresponds to a mechanism of deformation. As a whole, the above results demonstrate that the reverse plasticity and ratchet limits obtained by using the LMM framework are accurate.

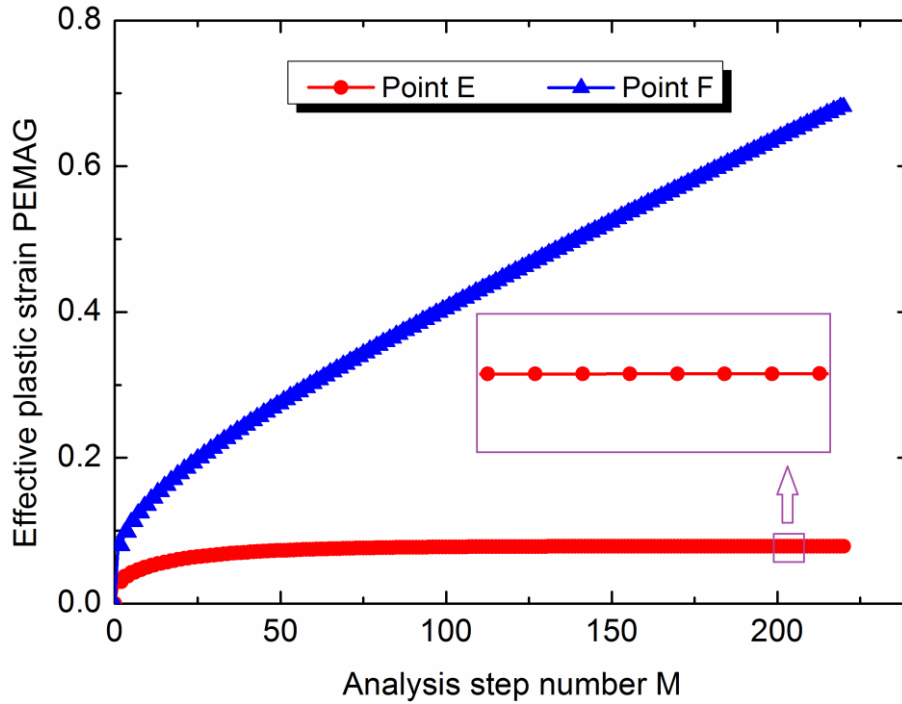
In following sections, we will mainly discuss the shakedown boundary (i.e. shakedown zone marked in Fig. 3) of the pressure pipeline with an oblique nozzle.



(a) Points A and B



(b) Points C and D



(c) Points E and F

Fig. 5 Relationship between the effective plastic strain and the number of cycles based on ABAQUS step-by-step analysis for various load cases

#### 4.2 Parametric studies on shakedown boundary

In this section, parametric studies on several factors affecting the shakedown boundary of the component are conducted, where the angle of the oblique nozzle, the diameter-to-thickness ratio of the oblique nozzle, the diameter-to-thickness ratio of the main pipe, and the fillet radius between the main pipe and the oblique nozzle, are considered for parametric studies.

##### 4.2.1 Angle of oblique nozzle

In this section, three typical angles of the oblique nozzle, i.e.,  $\varphi_0=45^\circ$ ,  $60^\circ$ , and  $90^\circ$ , are chosen for analyses, with the shakedown boundaries shown in Fig. 6. It can be observed that the angle of the oblique nozzle has a relatively small influence on the reverse plasticity limit of the component. However, the ratchet limit of the component is remarkably affected by the angle of the oblique nozzle. The increase of the angle of the oblique nozzle enhances the ratchet limit of the component.

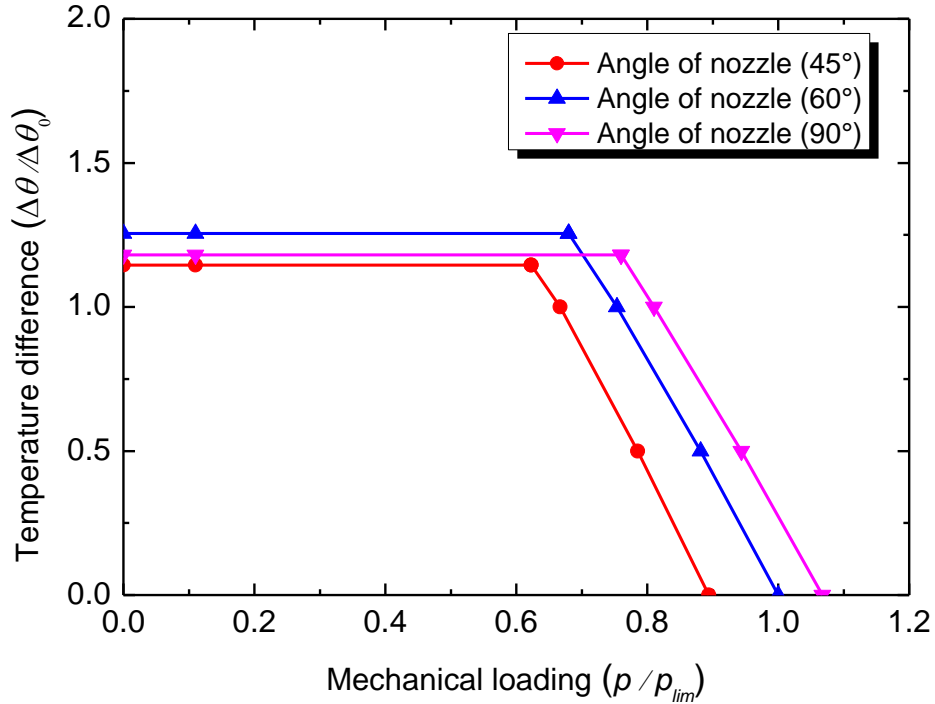


Fig. 6 Shakedown boundary curves of pressure vessel with an oblique nozzle for various angles of the oblique nozzle

The effective plastic strain distributions normalized to the maximum value for the component under the pure mechanical load case (i.e. the limit load) and under the cyclic thermal loading condition only (i.e. the reverse plasticity limit) for different angles of the oblique nozzle are displayed in Fig. 7 and Fig. 8, respectively. It can be seen that for the three angles of the oblique nozzle, the effective plastic strain for the pure mechanical loading cases is all concentrated at the joint of the main pipe and the nozzle, parallel to the axis of the main pipe. For the pure cyclic thermal loading condition, the effective plastic strains are still located at the joint between the main pipe and the oblique nozzle, but they present some differences (see Fig. 8). When a large angle is mentioned (i.e.  $\varphi_0=90^\circ$ ), the location with the maximum plastic deformation is perpendicular to the central axis of the main pipe, but this behavior is not applicable to small angles of the oblique nozzle (e.g.  $\varphi_0=45^\circ$  and  $60^\circ$ ). Exactly speaking, the maximum plastic strain for the angle of  $\varphi_0=45^\circ$  is at the inner surface of the model, while it is located at the outer surface of the joint for the angle of  $\varphi_0=60^\circ$ .

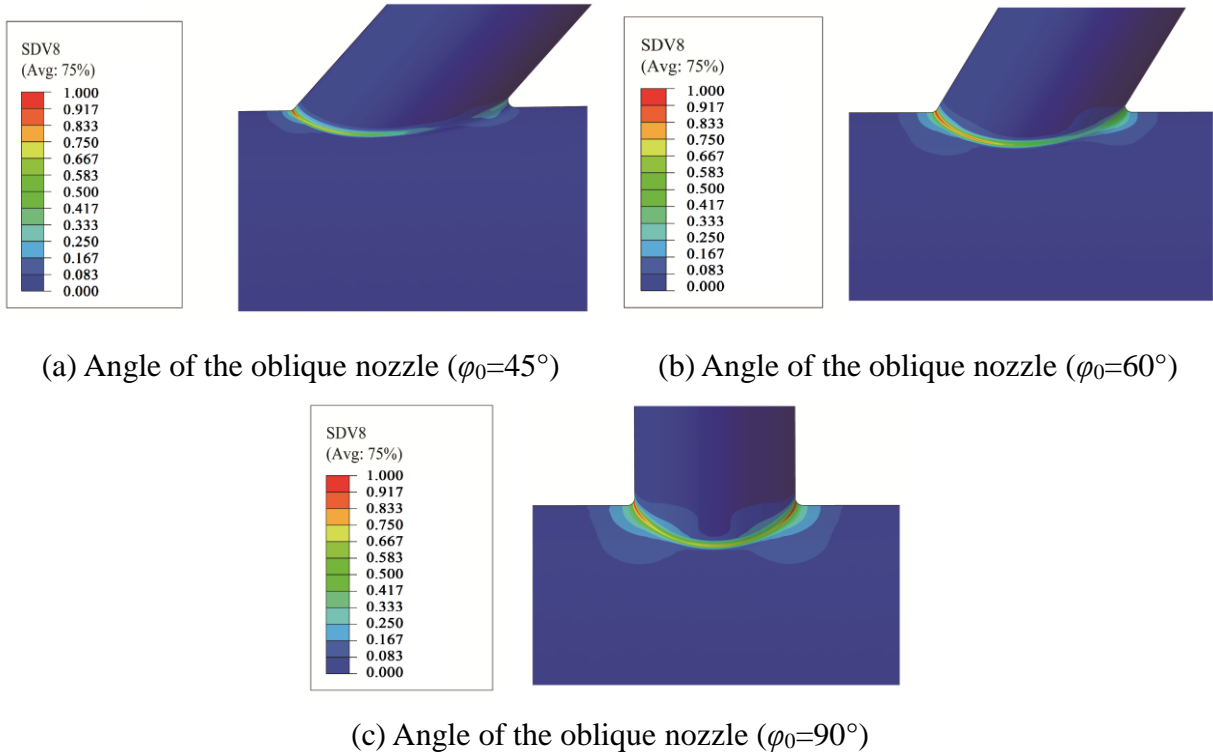


Fig. 7 Effective plastic strain distributions under pure mechanical loadings for various angles of the oblique nozzle

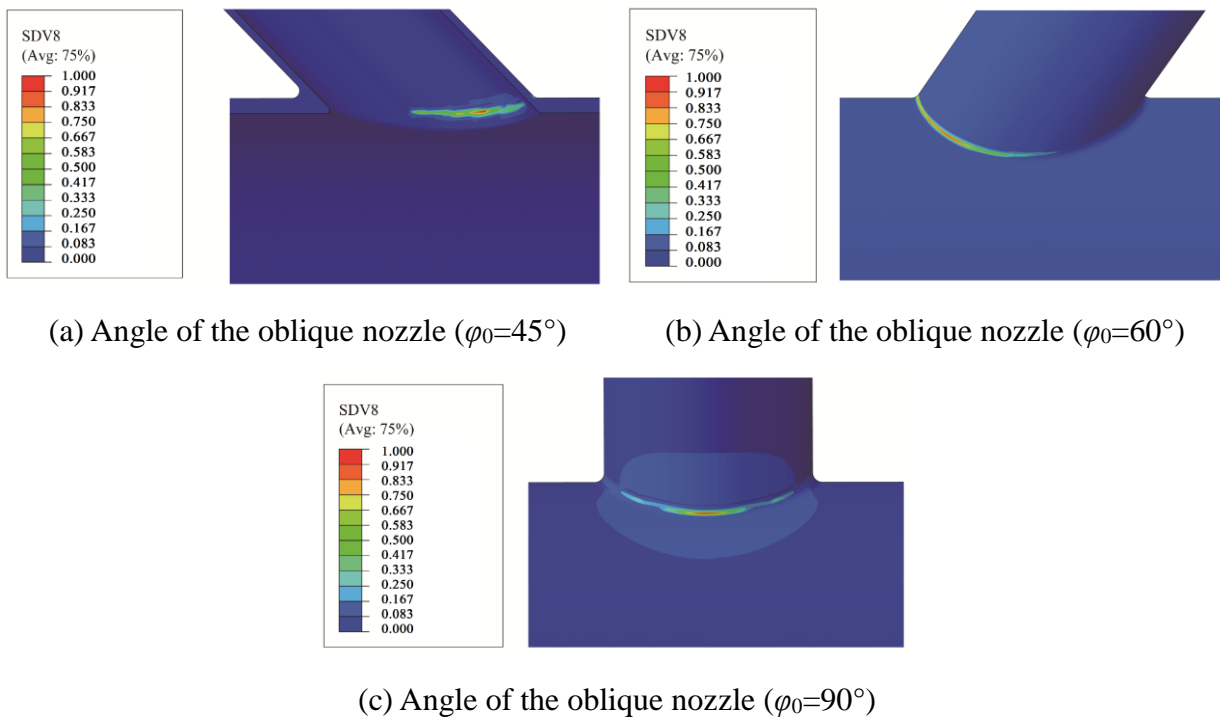


Fig. 8 Effective plastic strain distributions under pure thermal loadings for various angles of the oblique nozzle

#### 4.2.2 Diameter-to-thickness ratio of the oblique nozzle

The shakedown boundaries of the component with three diameter-to-thickness ratios of the oblique nozzle, i.e.,  $D_z/t_z=10.95$ , 21.9 and 43.8, are shown in Fig. 9. It can be indicated that the diameter-to-thickness ratio of the oblique nozzle can significantly affect the reverse plasticity and the ratchet limits. The increase of the diameter-to-thickness ratio can induce a remarkable decrease of the reverse plasticity and the ratchet limits of the component.

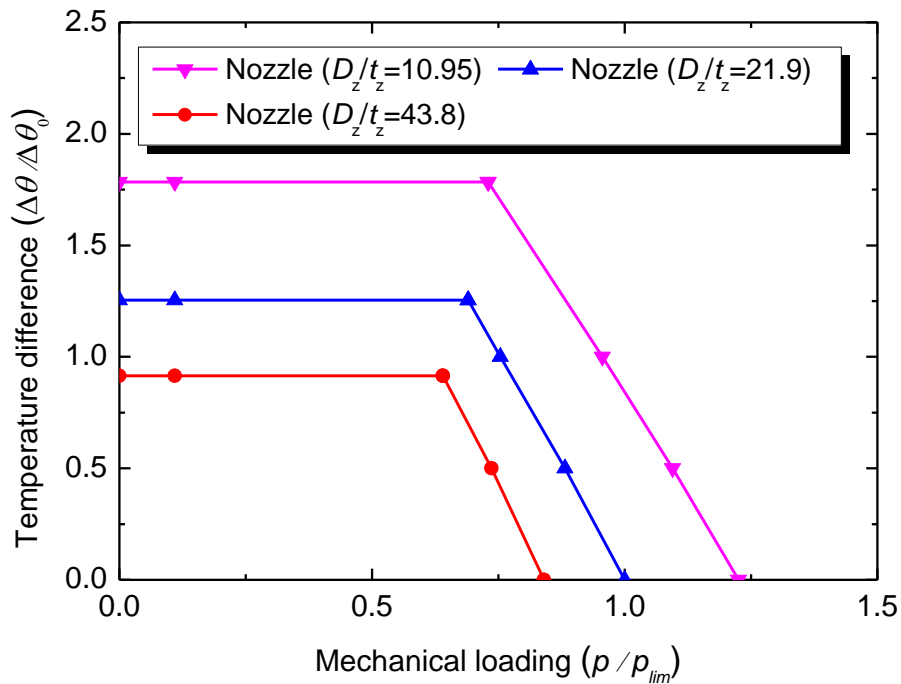
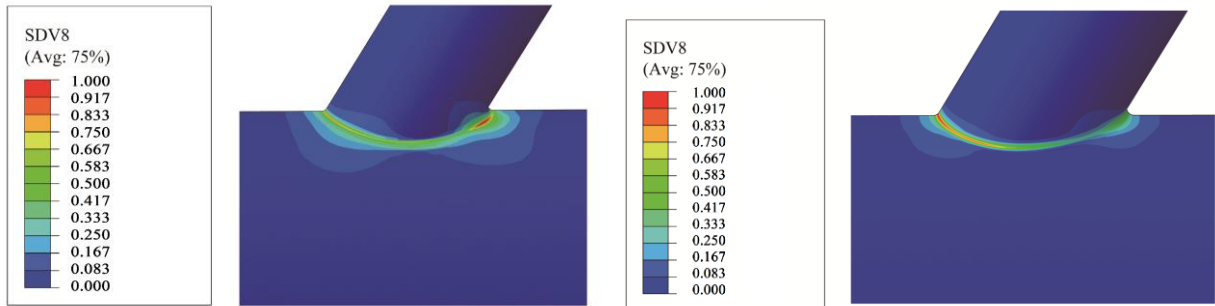


Fig. 9 Shakedown boundary curves of pressure vessel with an oblique nozzle for various diameter-to-thickness ratios of the oblique nozzle

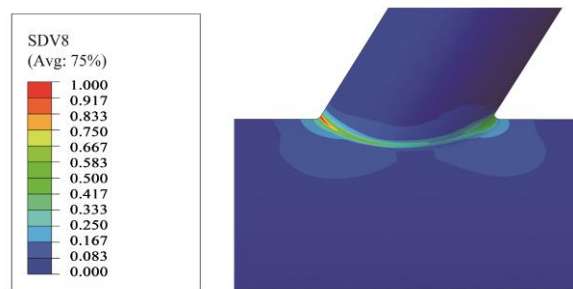
The effective plastic strain behaviors normalized to the maximum value for the component under the pure mechanical load case (i.e. the limit load) and under the cyclic thermal loading condition only (i.e. the reverse plasticity limit) for various diameter-to-thickness ratios of the oblique nozzle are displayed in Fig. 10 and Fig. 11, respectively. It can be seen that for the diameter-to-thickness ratios mentioned, the maximum effective plastic strain for the pure mechanical loading cases is all concentrated at the joint of the main pipe and the nozzle, parallel to the axis of the main pipe. For the pure cyclic thermal loading condition, the locations with the

maximum effective plastic strains for the above three diameter-to-thickness ratios indicate some differences. The maximum effective plastic strain is located at the inner surface of the joint for a high diameter-to-thickness ratio (e.g.  $D_z/t_z=43.8$ ), nearly parallel to the axis of the main pipe, while it is nearly perpendicular to the axis of the main pipe for a small diameter-to-thickness ratio (e.g.  $D_z/t_z=10.95$ ). This is induced by the thermal stress caused by the non-uniform temperature through the thickness in the vicinity of the joint between the main pipe and the oblique nozzle.



(a) Diameter-to-thickness ratio ( $D_z/t_z=10.95$ )

(b) Diameter-to-thickness ratio ( $D_z/t_z=21.9$ )



(c) Diameter-to-thickness ratio ( $D_z/t_z=43.8$ )

Fig. 10 Effective plastic strain distributions under pure mechanical loadings for various diameter-to-thickness ratios of the oblique nozzle

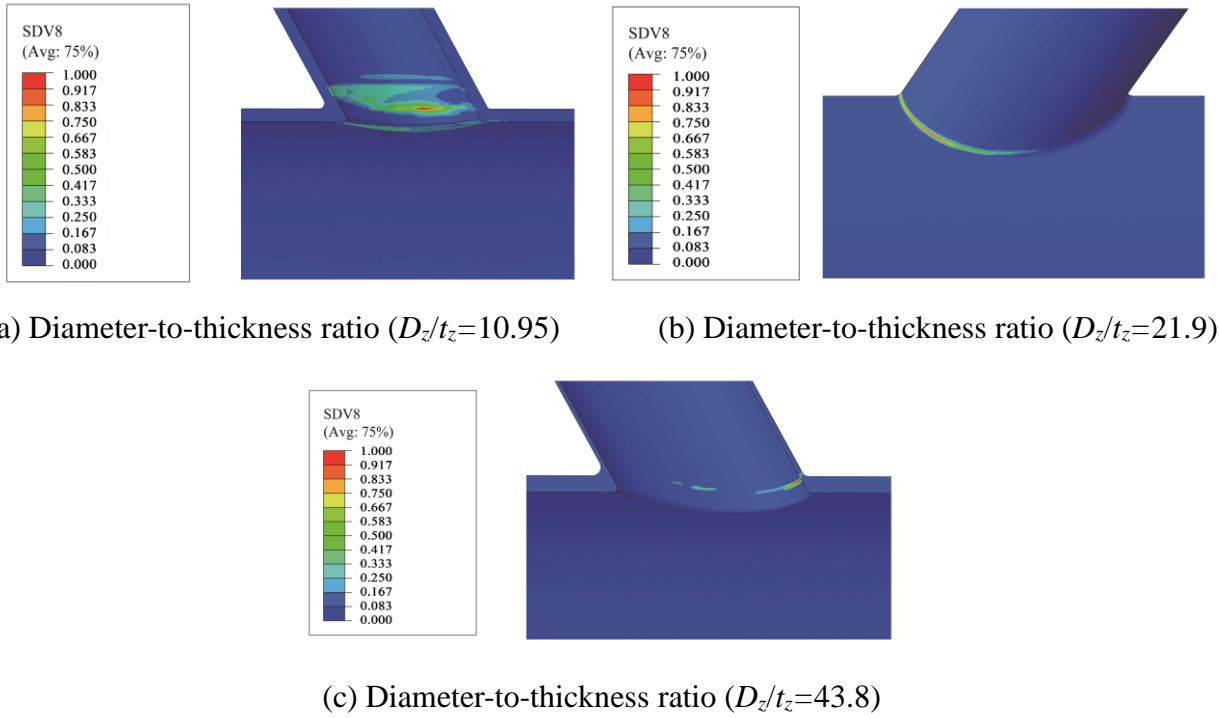


Fig. 11 Effective plastic strain distributions under pure thermal loadings for various diameter-to-thickness ratios of the oblique nozzle

#### 4.2.3 Diameter-to-thickness ratio of the main pipe

In this section, three diameter-to-thickness ratios of the main pipe, i.e.,  $D_p/t_p=8.73$ , 17.45 and 34.9, are adopted for calculations and the corresponding shakedown boundaries are shown in Fig. 12. It can be found that a large diameter-to-thickness ratio of the main pipe can induce a decrease of the ratchet limit greatly, but enhances the reverse plasticity limit remarkably.

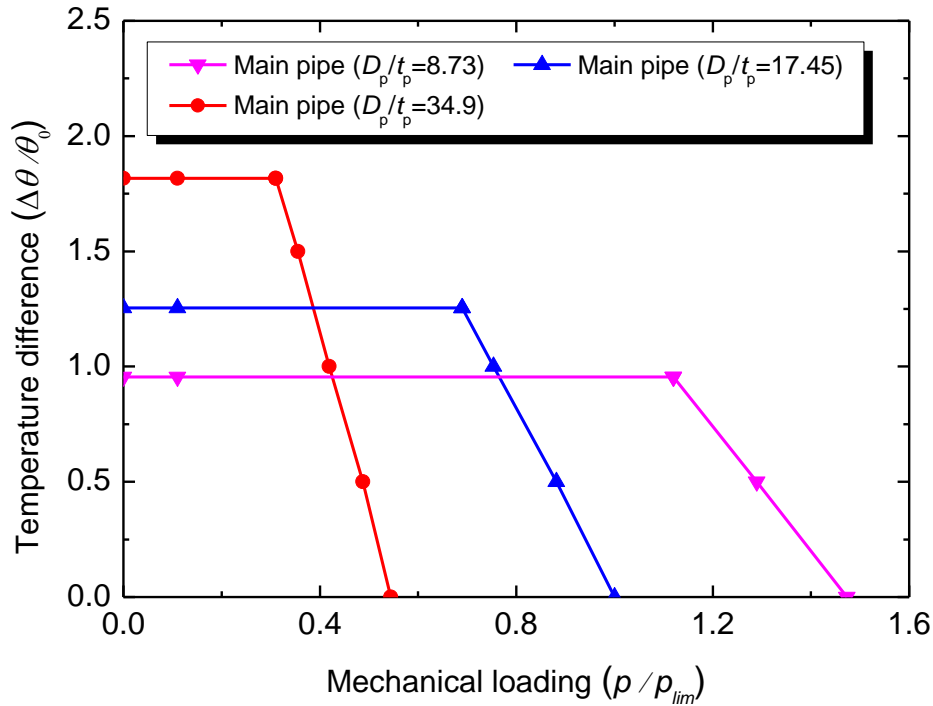
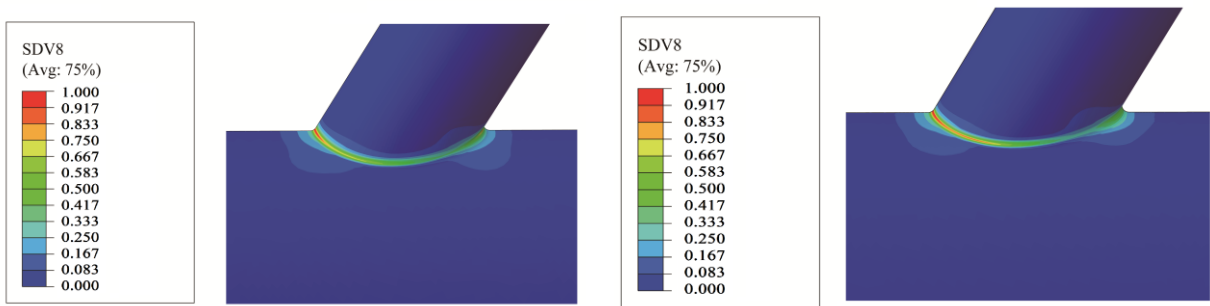


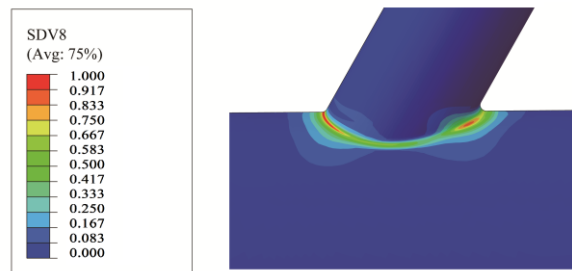
Fig. 12 Shakedown boundary curves of pressure vessel with an oblique nozzle for various diameter-to-thickness ratios of the main pipe

The effective plastic strain distributions normalized to the maximum value for the component under the pure mechanical load case (i.e. the limit load) and under the cyclic thermal loading condition only (i.e. the reverse plasticity limit) for various diameter-to-thickness ratios of the main pipe are displayed in Fig. 13 and Fig. 14, respectively. It can be found that for the three diameter-to-thickness ratios, the maximum effective plastic strain for the pure mechanical loading cases is located at the joint of the main pipe and the nozzle, parallel to the axis of the main pipe. For the pure cyclic thermal loading condition, the effective plastic strain distributions present some differences for three typical diameter-to-thickness ratios. The maximum effective plastic strain is mainly located at the inner surface of the main pipe for a high diameter-to-thickness ratio (e.g.  $D_p/t_p=34.9$ ), while it is on the outer surface of the joint for a small diameter-to-thickness ratio (e.g.  $D_p/t_p=8.73$  and  $17.45$ ). Similar to the factor (diameter-to-thickness ratio of the oblique nozzle) discussed in Section 4.2.2, the above difference may also result from the thermal stress due to the non-uniform temperature distribution around the joint between the main pipe and the oblique nozzle.



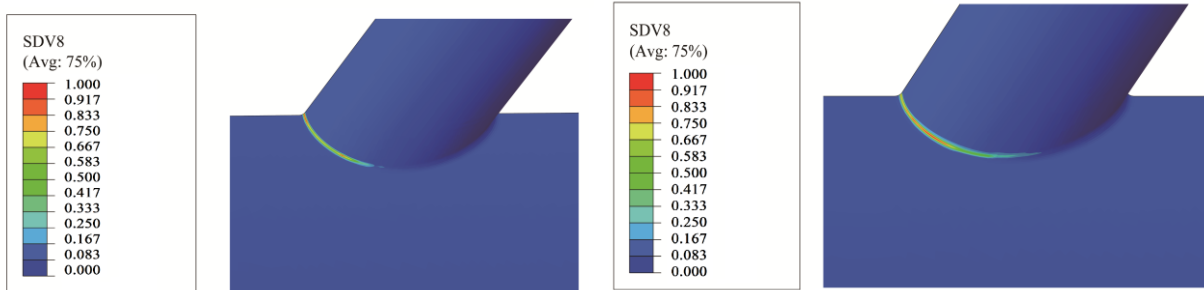
(a) Diameter-to-thickness ratio ( $D_p/t_p=8.73$ )

(b) Diameter-to-thickness ratio ( $D_p/t_p=17.45$ )



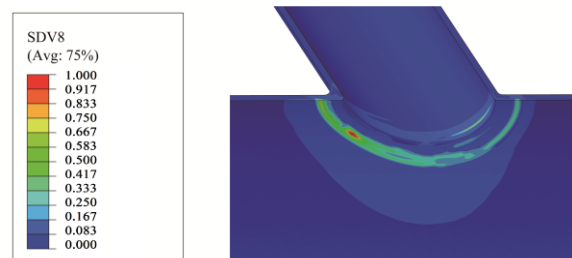
(c) Diameter-to-thickness ratio ( $D_p/t_p=34.9$ )

Fig. 13 Effective plastic strain distributions under pure mechanical loadings for various diameter-to-thickness ratios of the main pipe



(a) Diameter-to-thickness ratio ( $D_p/t_p=8.73$ )

(b) Diameter-to-thickness ratio ( $D_p/t_p=17.45$ )



(c) Diameter-to-thickness ratio ( $D_p/t_p=34.9$ )

Fig. 14 Effective plastic strain distributions under pure thermal loadings for various diameter-to-thickness ratios of the main pipe

#### 4.2.4 Fillet radius between main pipe and oblique nozzle

The shakedown boundaries for three fillet radius-to-nozzle thickness ratios, i.e.,  $R/t_z=0.5$ , 1.0 and 1.5, are displayed in Fig. 15. It should be noted that the fillet radius mentioned here is on the outer surface of the joint. It can be observed that the fillet radius has a slight effect on the reverse plasticity and ratchet limits of the component for all loading conditions mentioned. In addition, considering that the fillet radius does not manifest a remarkable difference on effective plastic strain distribution, so the corresponding strain distributions are not provided herein.

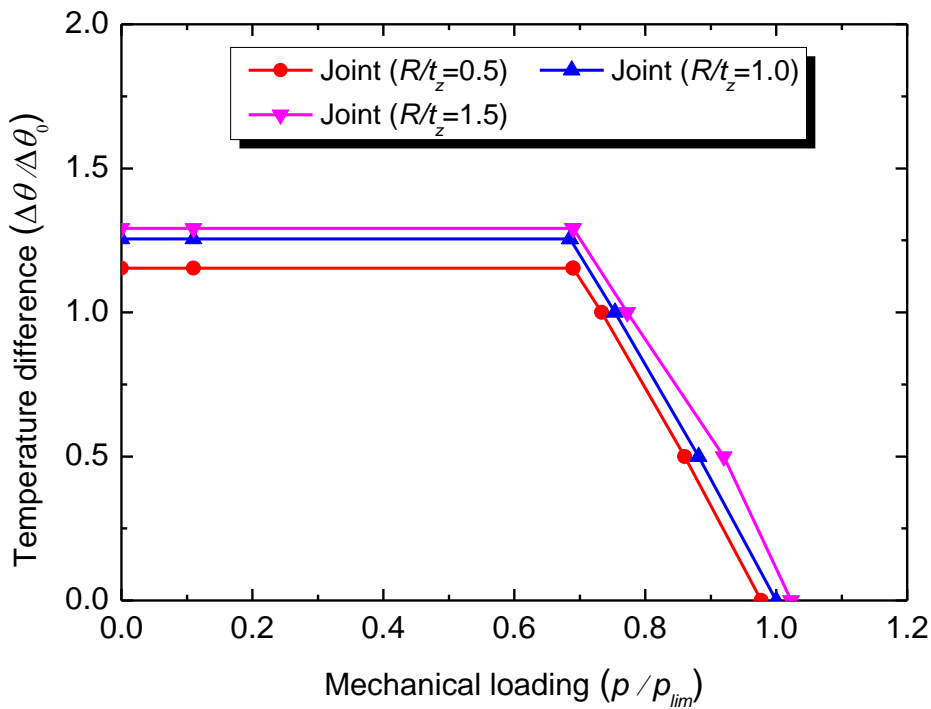


Fig. 15 Shakedown boundary curves of pressure vessel with an oblique nozzle for various fillet radiuses between the main pipe and the oblique nozzle

#### 4.3 Discussions

Through the above numerical analyses, it can be concluded that the angle of the oblique nozzle, the diameter-to-thickness ratios of the oblique nozzle and the main pipe are the main factors affecting the reverse plasticity and the ratchet limits of the component. Considering that the angle of the oblique nozzle is a representative variable, this factor will be mainly discussed in this section. In following, the effect of the angle of the oblique nozzle on shakedown boundaries (e.g. the limit load and the reverse plasticity limit) are employed for analyses.

The relationship between the limit load and the angle of the oblique nozzle is shown in Fig.

16a. The limit load of the component increases with the increase of the angle of the oblique nozzle, and then attains a steady limit load value. This demonstrates that the limit load is not sensitive to the angle of the oblique nozzle when the angle is higher than a certain value. In this case, the critical angle of the oblique nozzle is about  $\varphi_0=60^\circ$ . The equation describing the relationship between the limit load and the angle of the oblique nozzle is given as Eq. (16).

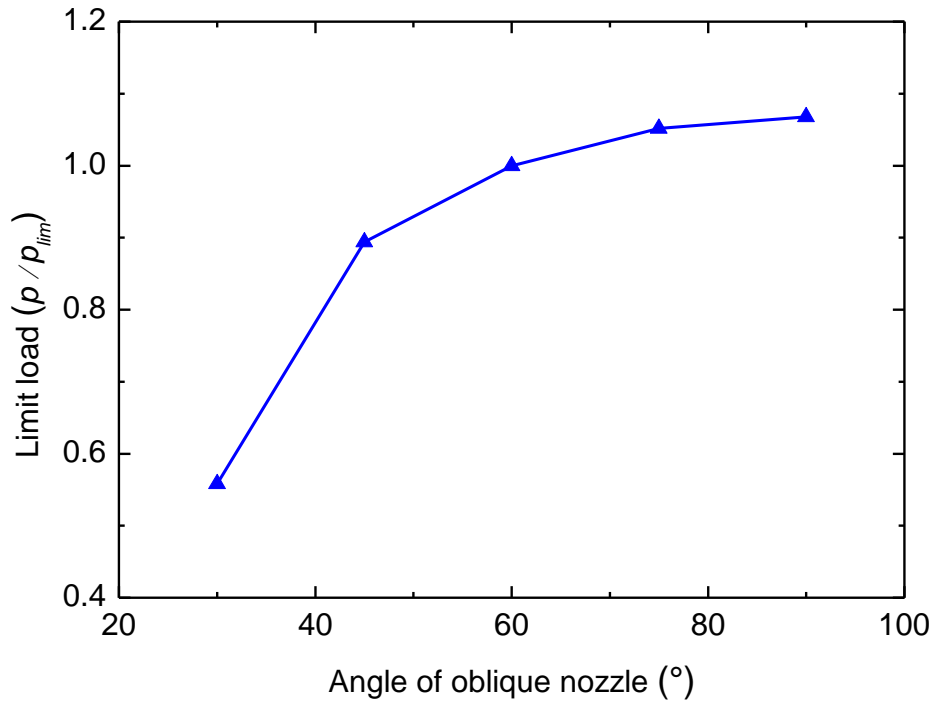
$$\frac{P}{P_{\text{lim}}} = f(\theta) = a_M \theta^2 + b_M \theta + c_M \quad (16)$$

where,  $a_M$ ,  $b_M$  and  $c_M$  are material constants, equal to  $-8.0 \times 10^{-5}$ , 0.0145 and 0.4036, respectively;  $P_{\text{lim}}$  is the limit internal pressure, equal to 9.369 MPa.

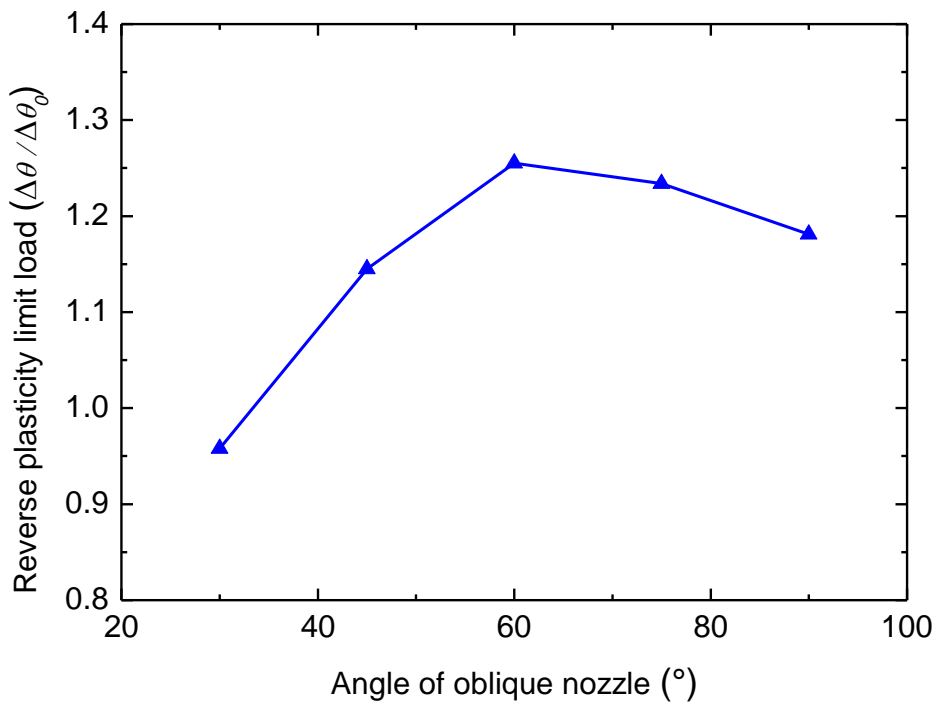
The relationship between the reverse plasticity limit and the angle of the oblique nozzle is given in Fig. 16b. The reverse plasticity limit of the component increases initially with the increase of the angle of the oblique nozzle, attains a maximum value at the angle of the oblique nozzle ( $\varphi_0=60^\circ$ ), and then presents a certain decrease. The above results illustrate that the component has a maximum reverse plasticity limit with the angle of the oblique equal to  $\varphi_0=60^\circ$ . The relationship between the reverse plasticity limit and the angle of the oblique nozzle is shown as Eq. (17).

$$\frac{\theta}{\theta_0} = f(\theta) = a_T \theta^2 + b_T \theta + c_T \quad (17)$$

where,  $a_T$ ,  $b_T$  and  $c_T$  are material constants, equal to  $-2.0 \times 10^{-4}$ , 0.0268 and 0.3296, respectively.  $\theta_0$  is the reference temperature difference, equal to  $100^\circ\text{C}$ . The above results also demonstrate that the designers should make some compromises on the limit load and reverse plasticity limit of the component when determining an economic angel of the oblique nozzle within a given range by the process design.



(a) Limit load



(b) Reverse plasticity limit

Fig. 16 Effect of the angle of oblique nozzle on limit load and reverse plasticity limit

## 5 Conclusions

In this work, the shakedown analysis of the pressure pipeline with an oblique nozzle at elevated temperatures is analyzed using the Linear Matching Method (LMM). Meanwhile,

parametric studies on main factors affecting the shakedown boundaries are conducted. The conclusions drawn through numerical investigations are summarized as follows:

(1) The current LMM software tool is successfully adopted to determine the Bree-like diagram (i.e. shakedown limit and ratchet limit) of the pressure pipeline with an oblique nozzle at elevated temperature. Numerical results are also verified by the ABAQUS step-by-step analysis.

(2) Parametric studies demonstrate that the diameter-to-thickness ratios of the oblique nozzle and the main pipe have a remarkable effect on the reverse plasticity and ratchet limit of the component. The angle of the oblique nozzle has a relatively significant effect on the ratchet limit, but has a relatively small influence on the reverse plasticity limit.

(3) The limit load of the component is enhanced with the increasing angle of the oblique nozzle, while the reverse plasticity limit increases with the angle of the nozzle until a maximum value is reached, and then presents a certain decrease. Designers should make some compromises on the limit load and the reverse plasticity limit when determining an economic angle of the oblique nozzle within a given range by the process design.

## **Acknowledgments**

The authors gratefully acknowledge the support of the University of Strathclyde, the East China University of Science and Technology, the Natural Science Foundation of China (Grants No.: 51475167, 51605165) and the 111 project during the course of this work.

## **References**

- [1] Koiter, W. T., 1960, "General Theorems for Elastic Plastic Solids," "Progress in Solid Mechanics", J. N. Sneddon, and R. Hill, eds., North Holland, Amsterdam, Vol. 1 , pp.167–221.
- [2] Melan, E., 1936, "Theorie Statisch Unbestimmter Systeme Aus Ideal-Plastischem Baustoff," Sitzungsber. d. Akad. d. Wiss., Wien 2A145 , pp.195–218.
- [3] Muscat, M., Mackenzie, D., and Hamilton, R., 2003, "Evaluating Shakedown by Non-Linear Static Analysis," *Comput. Struct.*, 81 , pp.1727–1737.
- [4] Vu, D. K., Yan, A. M., and Nguyen-Dang, H., 2004, "A Primal–Dual Algorithm for Shakedown

Analysis of Structures,” *Comput. Method Appl. Mech. Eng.*, 193 , pp.4663–4674.

- [5] Staat, M., and Heitzer, M., 2001, “LISA—A European Project for FEM-Based Limit and Shakedown Analysis,” *Nucl. Eng. Des.*, 206 , pp.151–166.
- [6] Seshadri, R., 1995, “Inelastic Evaluation of Mechanical and Structural Components Using the Generalized Local Stress Strain Method of Analysis,” *Nucl. Eng. Des.*, 153 (2–3), pp.287–303.
- [7] Mackenzie, D., Boyle, J. T., Hamilton, R., and Shi, J., 1996, “Elastic Compensation Method in Shell-Based Design by Analysis,” *Proceedings of the (1996) ASME Pressure Vessels and Piping Conference*, Vol. 338 , pp. 203–208.
- [8] Mackenzie, D., Boyle, J. T., and Hamilton, R., 2000, “The Elastic Compensation Method for Limit and Shakedown Analysis: A Review,” *Trans. IMechE J. Strain Anal. Eng. Des.*, 35 (3), pp.171–188.
- [9] Chen, H. F., and Ponter, A. R. S., 2001, “Shakedown and Limit Analyses for 3-D Structures Using the Linear Matching Method,” *Int. J. Pressure Vessels Piping*, 78 , pp.443–451.
- [10] Ponter, A. R. S., and Chen, H. F., 2001, “A minimum Theorem for Cyclic Loading in Excess of Shakedown, With Applications to the Evaluation of a Ratchet Limit,” *Eur. J. Mech. A/Solids*, 20 , pp.539–554.
- [11] Chen, H. F., and Ponter, A. R. S., 2001, “A Method for the Evaluation of a Ratchet Limit and the Amplitude of Plastic Strain for Bodies Subjected to Cyclic Loading,” *Eur. J. Mech., A/Solids*, 20 (4), pp.555–571.
- [12] Chen, H. F., and Ponter, A. R. S., 2005, “Integrity Assessment of a 3D Tubeplate Using the Linear Matching Method. Part 1. Shakedown, Reverse Plasticity and Ratchetting,” *Int. J. Pressure Vessels Piping*, 82 (2), pp.85–94.
- [13] Chen, H. F., and Ponter, A. R. S., 2006, “Linear Matching Method on the Evaluation of Plastic and Creep Behaviours for Bodies Subjected to Cyclic Thermal and Mechanical Loading,” *Int. J. Numer. Methods Eng.*, 68 , pp.13–32.
- [14] Chen, H. F., 2010, “A Direct Method on the Evaluation of Ratchet Limit,” *J. Pressure Vessel Technol.* 132 , 041202.
- [15] Chen, H., Ure, J., and Tipping, D. (2014), “Integrated structural analysis tool using the Linear

Matching Method part 2–Application and verification,” *International Journal of Pressure Vessels and Piping*, 120, pp.152-161.

- [16] Jackson, G. D., Chen, H. F., and Tipping, D. (2015), “Shakedown and creep rupture assessment of a header branch pipe using the Linear Matching Method,” *Procedia Engineering*, 130, pp.1705-1718.
- [17] Barbera, D., Chen, H., and Liu, Y. (2016), “Creep-fatigue behaviour of aluminum alloy-based metal matrix composite,” *International Journal of Pressure Vessels and Piping*, 139, pp.159-172.
- [18] Chen, H. (2010), “Linear matching method for design limits in plasticity,” *Computers, Materials and Continua-Tech Science Press*, 20(2), 159-183.
- [19] Abaqus User Manual. Dassault Systèmes Simulia Corp. 2009.
- [20] Siddall T. Finite Element Modelling and Shakedown Assessment of Cold Reheat Secondary Header Branches. EDF Energy Report E/REP/BBJB/0087/AGR/09, 2011.
- [21] Bree, J., 1989, “Plastic Deformation of a Closed Tube Due to Interaction of Pressure Stresses and Cyclic Thermal Stresses,” *Int. J. Mech. Sci.*, 31 (11–12), pp.865–892.